Dissipation in Laplacian fields across irregular boundaries

K. Karamanos and G. Nicolis
Centre for Nonlinear Phenomena and Complex Systems, Université Libre de Bruxelles, Campus Plaine, Code Postal 231, Boulevard du Triomphe, B-1050 Brussels, Belgium

T. Massart and P. Bouillard
Continuum Mechanics Department, Université Libre de Bruxelles, Code Postal 194/5, Avenue F. D. Roosevelt 50, B-1050 Brussels, Belgium

(Received 20 November 2000; published 26 June 2001)

The entropy production associated to a Laplacian field distributed across irregular boundaries is studied. In the context of the active zone approximation an explicit expression is given for the entropy production in terms of geometry, whose relation to the variational formulation is discussed. It is shown that the entropy production diminishes for successive prefractal generations of the same fractal generator, so that the final fractal object is expected to dissipate less than all previous ones. The relevance of this result in the abundance of fractal surfaces or interfaces observed in nature is discussed.

DOI: 10.1103/PhysRevE.64.011115 PACS number(s): 65.40.Gr, 05.70.Ln, 05.45.Df, 47.53.+n

I. INTRODUCTION

Recently, a number of studies on the role of the irregularity of a boundary in the spatial distribution of a field obeying Laplace's equation and of its associated flux has been reported. In particular, the case of fractal boundaries has been analyzed in depth using results from harmonic analysis along with extensive numerical computations based on finite element techniques [1–4].

One of the principal conclusions emerging from these studies is the existence of universal scaling laws culminating in the derivation of interesting expressions for the *impedance* describing the system's linear response. Many of these laws find their origin in Makarov's theorem stating that, whatever the shape of an irregular (simply connected) boundary in two dimensions might be, the *active zone* in which most of the flux generated by a Laplacian field is concentrated, scales as a length [5–7].

The relevance of the above results stems mainly from two factors. First, under ordinary conditions many familiar transport phenomena such as diffusion and heat conduction are described in the steady state by Laplacian fields [8]. And second, in nature as well as in technology the space in which these fields are distributed is far from regular. The terminal part of the respiratory system of mammals, biological membranes, porous electrodes or catalysts, provide some characteristic examples [8–14].

Our objective in the present study is to explore an alternative way to characterize the complexity of Laplacian transport across irregular boundaries, based on irreversible thermodynamics. More specifically we will be interested in the behavior of the *dissipation* generated by the underlying process, as the irregularity of the boundary is increased. Dissipation is here measured by the *entropy production*, arguably the central quantity of irreversible thermodynamics [15,16]. It has been shown that under the assumption of constant phenomenological coefficients linking the fluxes to the constraints this quantity satisfies a variational principle, thereby playing in nonequilibrium a role analogous to thermodynamic potentials in equilibrium. Curiously, as it will turn out, the range of validity of this result is incompatible with the Laplacian character of the associated field and, conversely, when this field is Laplacian entropy production no longer follows a variational principle. Nevertheless, it still provides an interesting characterization of nonequilibrium states, both locally in space and globally for the system as a whole. We shall see how the ''active zone'' concept allows one to incorporate in this characterization information pertaining to the geometry of the boundaries.

The general formulation is laid down in Sec. II. In Sec. III the entropy production associated to diffusion is evaluated within the active zone approximation for boundaries corresponding to the first two generations of an eventually fractal boundary. It is found that fragmentation tends to *decrease* both the total dissipation and the dissipation per unit surface. In Sec. IV the results are confronted with, and complemented by, those of numerical simulations. The main conclusions are summarized in Sec. V.

II. FORMULATION

Let ϕ be a scalar field associated to a conserved quantity. It is supposed that under the action of a nonequilibrium constraint this field gives rise to a single irreversible process whose flux $\mathbf{J}$ and the associated force $\mathbf{X}$ are vectors. While, typically, $\mathbf{X}$ is the space derivative of some function f of ϕ related to the derivative of a thermodynamic potential, $\mathbf{J}$ can be related to ϕ only through an appropriate phenomenological, or constitutive relation,

$$\mathbf{J}=L(\phi)\nabla f(\phi), \quad L>0, \tag{1}$$

where L is the (generally state-dependent) phenomenological or Onsanger coefficient. The field ϕ obeys, then, to a closed evolution equation of the form

$$\frac{\partial \phi}{\partial t}=-\operatorname{div}\mathbf{J}=-\operatorname{div}L(\phi)\nabla f(\phi), \tag{2}$$

it being understood that any extra factors in the left-hand side arising from thermodynamic derivatives (such as specific heat, etc.) have been absorbed in a suitably rescaled time.

The local entropy production associated with (1) and (2) is

$$\sigma = \mathbf{J}\cdot\mathbf{X} = L(\phi)(\nabla f(\phi))^2 \geqslant 0, \tag{3}$$

the overall dissipation being

$$P = \int_V \sigma d\mathbf{r}, \tag{4}$$

where V is the volume occupied by the system.

Let us assume first that L is strictly constant (state-independent). Equation (2) implies, then, that in the steady state $f(\phi)$ obeys Laplace's equation,

$$\operatorname{div}\nabla f(\phi) = \nabla^2 f(\phi) = 0. \tag{5}$$

Typically, the dependence of f on ϕ is nonlinear. For instance, in the diffusion of a solute in a solvent, say in an electrolytic cell, and in heat conduction in a slab one has, respectively,

$$f = -\frac{\mu}{T} \quad \text{(diffusion)}, \qquad f = \frac{1}{T} \quad \text{(heat conduction)}, \tag{6}$$

μ being the chemical potential and T the temperature. In an ideal mixture $\mu = \mu^* + kT\ln c$, c being the solute concentration, k the Boltzmann constant, and μ^* the standard chemical potential. It follows that the Laplacian fields associated to diffusion and heat conduction when L is constant are respectively, $\ln c$ and T^{-1} rather than c and T themselves. As shown in irreversible thermodynamics under the same assumptions, and provided that the boundary conditions are fixed or zero-flux ones, the total entropy production P is minimum at the steady state (Prigogine's theorem) [15,16],

$$P = L\int_V (\nabla f(\phi))^2 d\mathbf{r}. \tag{7}$$

To see this we differentiate both sides of Eq. (7) with respect to time,

$$\frac{\partial P}{\partial t} = 2L\int_V \nabla f(\phi)\cdot\nabla\frac{\partial f}{\partial t}d\mathbf{r} \tag{8}$$

or, integrating by parts and using the boundary conditions, Eq. (2) and the convexity of the thermodynamic potential,

$$\frac{\partial P}{\partial t} = 2\int_V \left(\frac{\partial f}{\partial \phi}\right)\left(\frac{\partial \phi}{\partial t}\right)^2 d\mathbf{r} \leqslant 0. \tag{9}$$

In real world systems L is rarely constant. More commonly it is, rather, a combination of L and ϕ that varies slowly in a certain relevant range of values of the state variables. Taking up our two examples of diffusion and heat conduction one has, for instance,

$$\mathbf{J} = -D\nabla c \quad \text{(Fick's law)}, \qquad D = \frac{kL}{c} \approx \text{const}, \tag{10}$$

and

$$\mathbf{J} = -\lambda\nabla T \quad \text{(Fourier's law)}, \qquad \lambda = \frac{L}{T^2} \approx \text{const} \tag{11}$$

It follows immediately from Eq. (2) that c and T are, then, Laplacian fields. As a counterpart, the entropy production loses its variational character. Below, we illustrate this in the case of diffusion, but the arguments apply to heat conduction as well. We have

$$P = \int_V (-D\nabla c)\cdot\nabla\left(\frac{-\mu}{T}\right)d\mathbf{r} \tag{12}$$

or, using the expression of μ for an ideal mixture introduced above,

$$P = Dk\int_V \frac{(\nabla c)^2}{c}d\mathbf{r}. \tag{13}$$

Hence,

$$\frac{\partial P}{\partial t} = Dk\int_V \frac{-1}{c^2}\frac{\partial c}{\partial t}(\nabla c)^2 d\mathbf{r} + 2Dk\int_V \frac{1}{c}(\nabla c)\cdot\nabla\left(\frac{\partial c}{\partial t}\right)d\mathbf{r}. \tag{14}$$

Integrating again by parts and using the boundary conditions and the diffusion equation one has

$$\frac{\partial P}{\partial t} = -2k\int_V \frac{1}{c}\left(\frac{\partial c}{\partial t}\right)^2 d\mathbf{r} + Dk\int_V \frac{(\nabla c)^2}{c^2}\frac{\partial c}{\partial t}d\mathbf{r}. \tag{15}$$

While the first term is negative definite, the second one has no definite sign: dissipation no longer derives from a variational principle. On the other hand, following a procedure similar to the one leading to Eq. (9), one easily sees that the functional

$$Q = \int_V (\nabla c)^2 d\mathbf{r} \tag{16}$$

is extremal in the steady state [17].

In the sequel we will be interested in the behavior of P as given by Eq. (13) under the condition that, as stated above, c satisfies in the steady state Laplaces's equation

$$\nabla^2 c = 0. \tag{17}$$

Before we address the role of complex boundaries we evaluate both c and P in the simple reference case of a two-dimensional box of height L_y and length L_x submitted to Dirichlet conditions along the y direction and to zero-flux ones along the x direction. The solution of Eq. (17) is then trivially given as a linear concentration profile

$$c(y)=\frac{c_1-c_2}{L_y}y+c_2, \tag{18}$$

where $c_1=c(L_y)$, and $c_2=c(0)$. The entropy production can be calculated exactly, yielding

$$P=Dk\frac{L_x}{L_y}(c_2-c_1)\ln\frac{c_2}{c_1}. \tag{19}$$

We notice that P diverges for the absorbing boundary condition $c_2=0$ on $y=0$. For fixed c_1 and c_2 it is inversely proportional to the size L_y. On the other hand, for fixed gradient $\beta=(c_2-c_1)/L_y$ one has

$$P=Dk\beta L_x\ln\left(1+\frac{\beta L_y}{c_1}\right).$$

For $\beta L_y/c_1\ll 1$ this expression further reduces to

$$P=DkL_xL_y\frac{\beta^2}{c_1}, \tag{20}$$

featuring now a dependence proportional to the system size. This reflects the extensivity of entropy production.

Continuing along the same lines, one can readily perform the integration in Eq. (16), leading to the following expression for the variational functional in terms of geometry

$$Q=\frac{L_x}{L_y}(c_2-c_1)^2=L_xL_y\beta^2. \tag{21}$$

Notice that unlike the entropy production [Eq. (19)], the variational functional no more diverges for the absorbing boundary condition $c_2=0$ on $y=0$ usually adopted in the literature.

III. IRREGULAR BOUNDARIES: ANALYTIC APPROACH

The simplest setting in which possible effects of complex geometry on entropy production can be identified is given in Fig. 1. A concentration difference c_1-c_2 is applied across the vertical boundaries of a cell, over a characteristic length L_y. The cell obeys to zero-flux boundary conditions along the horizontal direction x, but there is now an anomaly consisting of extending the horizontal characteristic length L_x by a bump in the middle. An essential feature of the Laplacian field is to diverge in the corners created by this bump and this makes the treatment of the problem nontrivial. These singularities are, however, integrable (see [1–3]).

The most straightforward guess on entropy production is that it would keep the structure of Eq. (19) as far as y dependence goes, but the proportionality factor L_x would be modulated on the grounds of Makarov's theorem by an additional

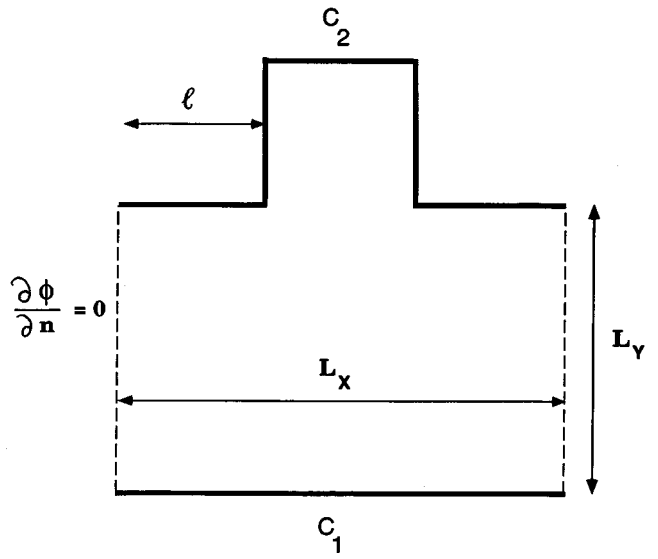

FIG. 1. Schematic representation of the diffusion cell for the first fractal iteration of a fractal generator. The dimensions of the cell as well as the boundary conditions are also indicated.

size-independent factor A depending on geometry and on concentrations only:

$$P=DkA(c_1,c_2;g)L_x\frac{1}{L_y}(c_2-c_1)\ln\frac{c_2}{c_1}. \tag{22}$$

Under the same conditions the variational functional Q should have the form

$$Q=B(g)L_x\frac{1}{L_y}(c_2-c_1)^2, \tag{23}$$

where now the constant B depends on geometry only.

Clearly, $A(c_1,c_2;g)=1$ and $B(g)=1$ for a flat membrane [cf. Eqs. (19) and (21)]. As it will turn out, $A(c_1,c_2;g)<1$ and $B(g)<1$ for a nonflat surface owing to the curvature of the equipotential lines arising from the geometric irregularities of the membrane. This means that a system bounded by an irregular membrane possesses the same entropy production as a smaller system with regular boundary conditions.

To estimate A and B we apply the active zone concept. We first observe that there are connections between these quantities. In the case of *mild diffusion*, $|(c_2-c_1)/c_1|=O(\varepsilon)$, $\varepsilon\ll 1$, with $c_1=O(1)$, we have from Eqs. (20) and (21) that

$$P\approx\varepsilon^2 \tag{24}$$

and

$$Q\approx\varepsilon^2. \tag{25}$$

Furthermore,

$$B(g)\approx\lim_{c_2\to c_1}A^{\mathrm{mild}}(c_1,c_2;g) \tag{26}$$

up to a factor of Dk/c_1.

The situation may be very different for *strong diffusion*, $|(c_2-c_1)/c_1|=O(1)$, $c_1=O(1)$. As the previous arguments cannot be applied straightforwardly, this case can only be analyzed numerically, as seen in detail in Sec. IV.

In the remaining part of this section we focus on the case of *mild diffusion*. Our purpose is to estimate B and A analytically in this limit. To this end we follow the ''independent field approximation'' (IFA). This is a coarse-graining argument based on a compartmentalization of the full continuous space in which diffusion takes place into a finite number of properly selected nonoverlapping and noninteracting rectangular regions, where one can write down closed expressions for the entropy production and the variational functional supposing linear concentration profiles. The nonlinearity of the field arising from the irregularities of the boundaries is thus approximated by piecewise linear functions, entailing discontinuities of the equipotential lines at the boundaries between the cells.

Let us illustrate how the IFA works for the first fractal generation of the cell (Fig. 2) and for three geometries (a)–(c) corresponding to three different depths. We separate the cell into the three rectangles shown in the figure. Accepting linear concentration profiles in each of the side parts (i) and (iii), one finds for the entropy production, applying Eq. (19) with $L_x=l$ and $L_y=l$

$$P^{(\mathrm{i})}=P^{(\mathrm{iii})}=Dk(c_2-c_1)\ln\frac{c_2}{c_1}. \tag{27}$$

Accepting furthermore a linear half penetration inside the pore (that is, a linear concentration profile until the middle of the pore [2], thereby neglecting the remaining passive zone), one has for the central region (ii) from Eq. (19) with $L_x=l$ and $L_y=3l/2$

$$P^{(\mathrm{ii})}=\tfrac{2}{3}Dk(c_2-c_1)\ln\frac{c_2}{c_1}. \tag{28}$$

The total entropy production of the cell becomes

$$P^{\mathrm{tot}}=P^{(\mathrm{i})}+P^{(\mathrm{ii})}+P^{(\mathrm{iii})}=\tfrac{8}{3}Dk(c_2-c_1)\ln\frac{c_2}{c_1}. \tag{29}$$

Applying now Eqs. (22) and (26) for the whole cell with $L_x=3l$ and $L_y=l$ we find [remember that we deal here with mild diffusion, see Eq. (26)]

$$P^{\mathrm{tot}}=3DkB(g)(c_2-c_1)\ln\frac{c_2}{c_1}. \tag{30}$$

Comparison with Eq. (22) leads to

$$3B(g)=\tfrac{8}{3}, \tag{31}$$

that is,

$$B_a^{(1)}=\tfrac{8}{9}\cong 0.889 \tag{32}$$

for geometry (a). Continuing in the same manner one finds

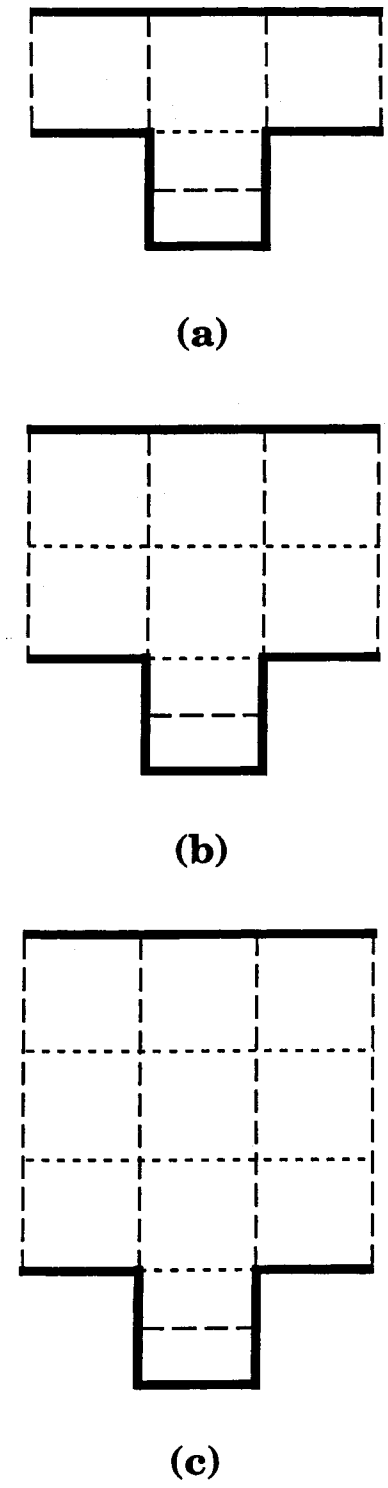

FIG. 2. Schematic representation of the coarse-graining procedure associated with the IFA, for geometries (a), (b), and (c) of the first fractal iteration of a fractal generator.

$$B_b^{(1)}=\tfrac{14}{15}\cong 0.933 \tag{33}$$

for geometry (b) and

$$B_c^{(1)}=\tfrac{20}{21}\cong 0.952 \tag{34}$$

for geometry (c).

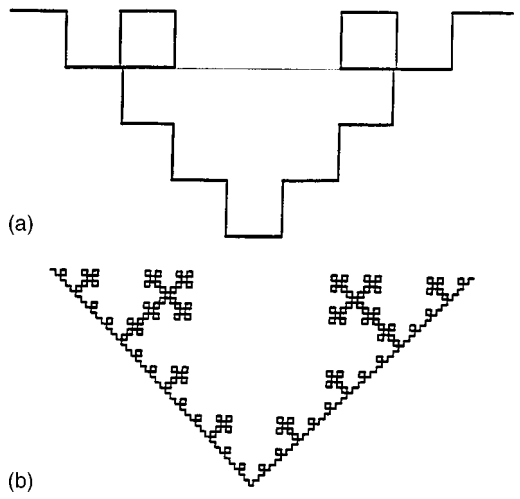

FIG. 3. The second (a) and the fourth (b) fractal iterations of the fractal generator used in our study.

For the second fractal iteration [Fig. 3(a)] one finds proceeding along similar lines

$$B_a^{(2)}=\tfrac{6}{7}\cong 0.857 \tag{35}$$

for geometry (a),

$$B_b^{(2)}=\tfrac{536}{585}\cong 0.916 \tag{36}$$

for geometry (b) and

$$B_c^{(2)}=\tfrac{1126}{1197}\cong 0.941 \tag{37}$$

for geometry (c).

Finally, for the third fractal iteration one finds

$$B_a^{(3)}=\tfrac{3050}{3591}\cong 0.849 \tag{38}$$

for geometry (a),

$$B_b^{(3)}=\tfrac{59236}{64935}\cong 0.912 \tag{39}$$

for geometry (b), and

$$B_c^{(3)}=\tfrac{185258}{197505}\cong 0.938 \tag{40}$$

for geometry (c).

Although crude, this evaluation gives some insight on the physical origin of $B(g)$. On the other hand, the argument of half-penetration of the field in the pore is expected to hold better when the distance of the source of particles from the entrance of the pore is larger than the depth of the geometrical irregularity. One thus expects an improvement of the quality of the predictions from geometry (a) to (c), a fact that is confirmed numerically.

On inspecting the above calculated coefficients $B^{(k)}$, one sees that they diminish from one fractal iteration to the next one. This turns out to be a general feature, implying that the coefficients $B^{(k)}$ are ordered

$$B^f<\cdots<B^{(k+1)}<B^{(k)}<\cdots<B^{(2)}<B^{(1)}<1. \tag{41}$$

Following the IFA argument and referring to Eq. (22), we may thus conclude that the entropy production diminishes from one fractal generation to the next, so that the final fractal object is expected to dissipate less than all previous ones. This is an important *least entropy production* statement in respect to *geometry*. This statement has some very interesting consequences from a physical point of view as discussed in Sec. V.

Notice finally that the entropy production [Eq. (13)] remains invariant under a *homothecy* transformation of all the lengths $L_x\rightarrow\lambda L_x$, $L_y\rightarrow\lambda L_y$ in two dimensions, as one sees from Eq. (22). In particular, no characteristic length scale subsists in the expression for the entropy production.

IV. IRREGULAR BOUNDARIES: NUMERICAL APPROACH

The Laplace equation for geometries associated with the first and the second fractal generations has been solved numerically using a general mechanical purpose Finite Element code SAMCEF.

Both geometries were discretized using linear three-noded triangular elements [19]. The continuity of the shape functions allowed one to apply a linear interpolation of the potential field and a constant value of its gradient on a given element and thereby a piecewise constant approximation of its gradient.

The characteristics of the meshes used in the computations are listed in the table below.

Generation	No. of nodes	No. of elements
1	10 327	20 052
2	10 342	20 128

The global entropy production was then computed for various boundary conditions by integrating the local entropy production obtained from the field and the associated flux (essentially its gradient). This quadrature was implemented using a 25-integration points scheme derived by Laursen and Gellert [20].

Figures 4(a), 4(b) and 5(a), 5(b) depict the spatial dependence of the entropy production, for the first and the second fractal generation and for boundary conditions corresponding, respectively, to strong and to mild diffusion. From these plots it is evident that the active zone concept is an excellent approximation in the case of mild diffusion, but becomes less sharp as one switches to the regime of strong diffusion. We also see the appearance of ''hot spots'' of dissipation near the bumps that are localized for the first fractal generation, and more extended for the second. They follow an analogous enhancement known to occur for the flux [1–3]. This enhancement is strengthened further in the case of strong diffusion by the factor c^{-1} in Eq. (13), which tends to increase in this region because of the boundary conditions. We recall that this is precisely the regime in which the entropy production P and the variational functional Q become clearly differentiated.

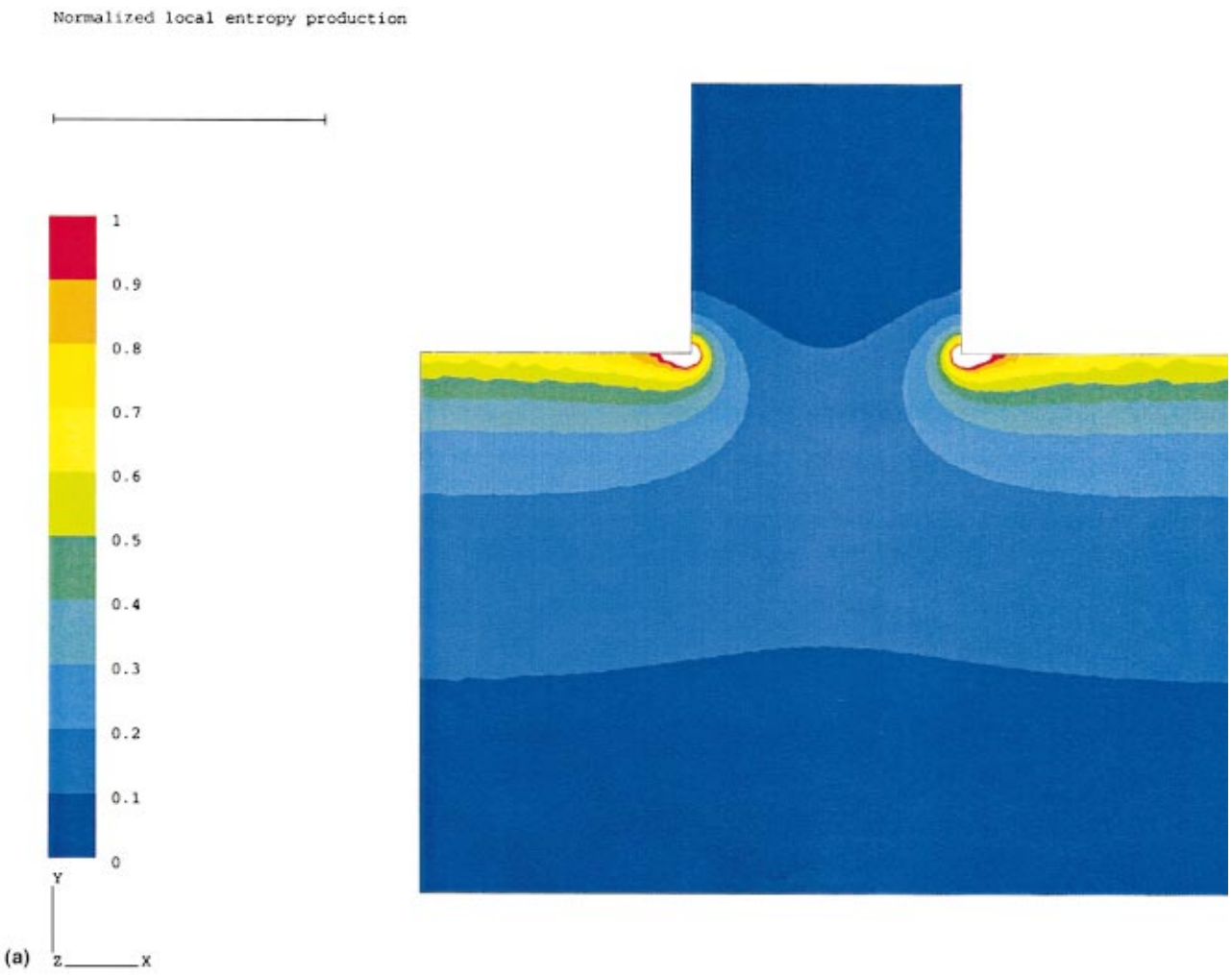

FIG. 4. (Color) Spatial dependence of the normalized entropy production for the diffusion cell of Fig. 1, for the cases of *strong* (a) ($c_2=0.1$) and *mild* (b) ($c_2=0.9$) diffusion. Computer units.

An additional interesting feature in the regime of strong diffusion is a more pronounced spatial differentiation of local entropy production reflected, in particular, by the appearance of a second inactive zone of negligible dissipation situated near the lower boundary [Figs. 4(a) and 5(a)].

The variation of entropy production normalized by Dk/c_1 (full lines) and of the variational functional (dotted lines) as a function of the concentration c_2 in the upper boundary is given in Fig. 6 for the first fractal generation. The following trends are worth stressing.

(i) P and Q decrease systematically as one tends to the regime of mild diffusion.

(ii) As c_2 tends to the value of the concentration in the regular boundary ($c_1=1$), the values of P and Q become indistinguishable.

Table I depicts the variation of the entropy production as a function of the concentration c_2 in the upper boundary for the first and the second fractal generations. As can be seen, the values for the entropy production corresponding to the second generation lie everywhere below those corresponding to the first generation. The number in square brackets indicates the power of ten.

The scaling factors $A(c_1,c_2;g)$ and $B(g)$ follow a similar trend, except that A *increases* toward the value B as one approaches the regime of mild diffusion, in accordance with the active zone concept valid in this latter limit.

Using the above results one may estimate the factor B with a very good precision (up to three significant digits). One obtains

$$B_a^{(1)\mathrm{ph}} \cong 0.949 \tag{42}$$

for geometry (a),

$$B_b^{(1)\mathrm{ph}} \cong 0.974 \tag{43}$$

for geometry (b),

$$B_c^{(1)\mathrm{ph}} \cong 0.982 \tag{44}$$

for geometry (c), where the superscript ''ph'' stands for ''phenomenological.'' Comparing with Eqs. (32)–(34), we see that $B_a^{(1)}$ differs from $B_a^{(1)\mathrm{ph}}$ by 6%, $B_b^{(1)}$ differs from $B_b^{(1)\mathrm{ph}}$ by 4% and $B_c^{(1)}$ differs from $B_c^{(1)\mathrm{ph}}$ by 4%.

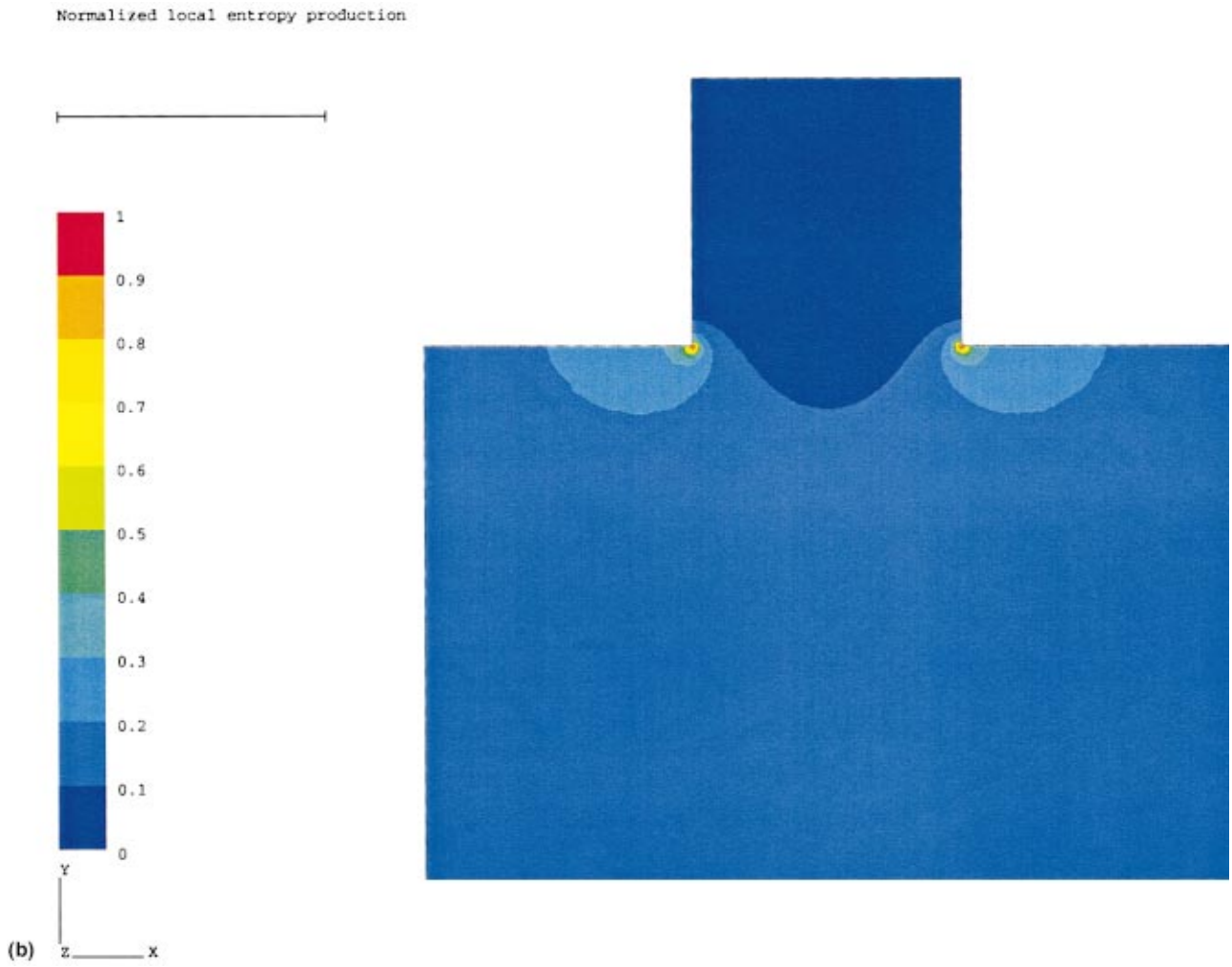

FIG. 4. (*Continued*).

These values differ significantly from the corresponding constant α, which appears in the expression

$$Z_{\mathrm{Mak}}=\frac{r_s}{\alpha L_x \rho} \tag{45}$$

for the impedance of an electrode or membrane in the Makarov regime [3], where r_s is the Faradaic resistance, which describes the rate of the electrochemical surface reaction and ρ is the electrolyte resistivity of the bulk. For instance,

$$\alpha^{(1)\mathrm{ph}} \simeq 0.87 \tag{46}$$

and this value corresponds essentially to $L_y \to \infty$. The above results have been further confirmed by calculations using a finite difference scheme [3,17,18].

The finite element method also gave us the values of B for the second generation

$$B_a^{(2)\mathrm{ph}} \simeq 0.937 \tag{47}$$

for geometry (a),

$$B_b^{(2)\mathrm{ph}} \simeq 0.967 \tag{48}$$

for geometry (b), and

$$B_c^{(2)\mathrm{ph}} \simeq 0.978 \tag{49}$$

for geometry (c).

Inserting the phenomenological (numerical) values for the coefficients $B_i^{(1)}$, one can actually obtain a ''renormalized'' value for the higher-order coefficients $B_i^{(2)}$ etc., thus improving considerably the predictions of the theory. Combining the empirical result for the first generation with a IFA half-penetration argument inside the new pores for the second fractal generation, one easily finds

$$B_a^{(2)\mathrm{ren}} = \left(0.949 - \frac{2}{3}\right) + \frac{40}{21} \simeq 0.918 \tag{50}$$

for geometry (a),

$$B_b^{(2)\mathrm{ren}} \cong 0.957 \tag{51}$$

for geometry (b), and

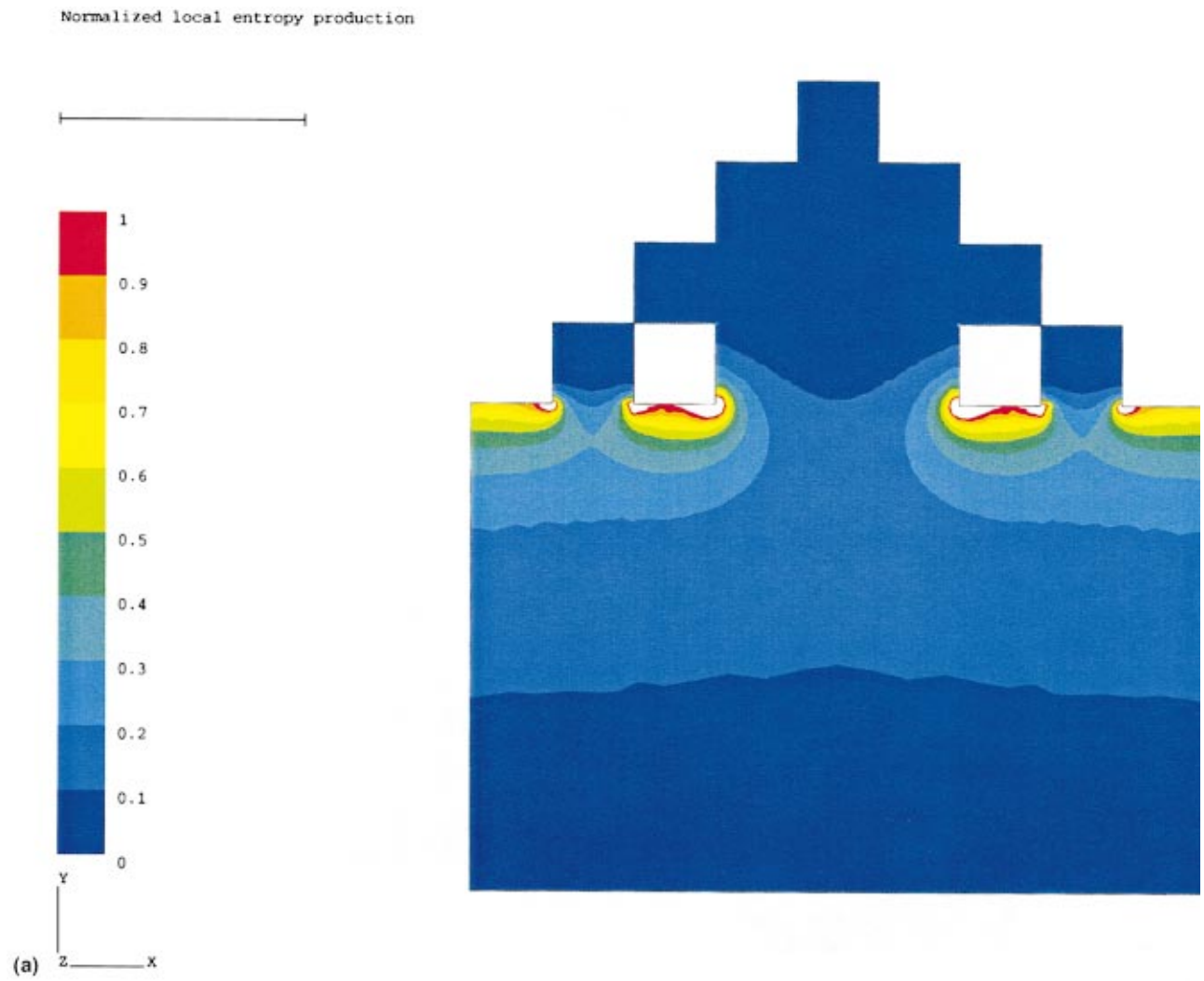

FIG. 5. (Color) Spatial dependence of the normalized entropy production for the diffusion cell of the second fractal iteration, for the cases of *strong* (a) ($c_2=0.1$) and *mild* (b) ($c_2=0.9$) diffusion. Computer units.

$$B_c^{(2)\mathrm{ren}} \cong 0.970 \tag{52}$$

for geometry (c).

One can try various renormalization schemes together with theoretical arguments. The best results are obtained when one uses for the prediction of the coefficient of the $k+1$ fractal iteration $B^{(k+1)}$ only the empirical coefficients of the previous k iteration and no theoretical argument at all. This is for instance the case of the second fractal iteration of geometry (a) for which we find

$$B_a^{(2)\mathrm{fren}} = (0.949 - \tfrac{2}{3}) + \tfrac{2}{3} \times 0.982 \cong 0.937, \tag{53}$$

where the superscript ''fren'' stands for ''fully renormalized.''

Comparing these results we find that $B_b^{(2)}$ differs from $B_b^{(2)\mathrm{ph}}$ by 5% and $B_b^{(2)\mathrm{ren}}$ differs from $B_b^{(2)\mathrm{ph}}$ by only 1%, while $B_c^{(2)}$ differs from $B_c^{(2)\mathrm{ph}}$ by 4% and $B_c^{(2)\mathrm{ren}}$ differs from $B_c^{(2)\mathrm{ph}}$ by less than 0.8%, which is in quite impressive agreement with the predictions of the theory.

V. CONCLUSIONS

In this paper the dissipation associated with a Laplacian field, as measured by the entropy production, has been studied for geometries associated with the first few generations leading eventually to a fractal boundary.

An analytic procedure based on the active zone concept was first applied. It led to the conclusion that as the boundary fragmentation is increasing, the total entropy production and, *a fortiori*, the entropy production per unit surface are decreasing. As the validity of this procedure is guaranteed only in the regime of mild diffusion, extensive numerical computations were also carried out. The results have fully corroborated the analytic evaluations in the mild diffusion case and provided detailed information on the strong diffusion case as well, in which entropy production does not coincide with the variational functional from which the Laplacian field is deriving.

The conclusion that dissipation tends to decrease with fragmentation is at first sight surprising, since fragmentation tends to create ''hot spots'' in which the flux—and hence the

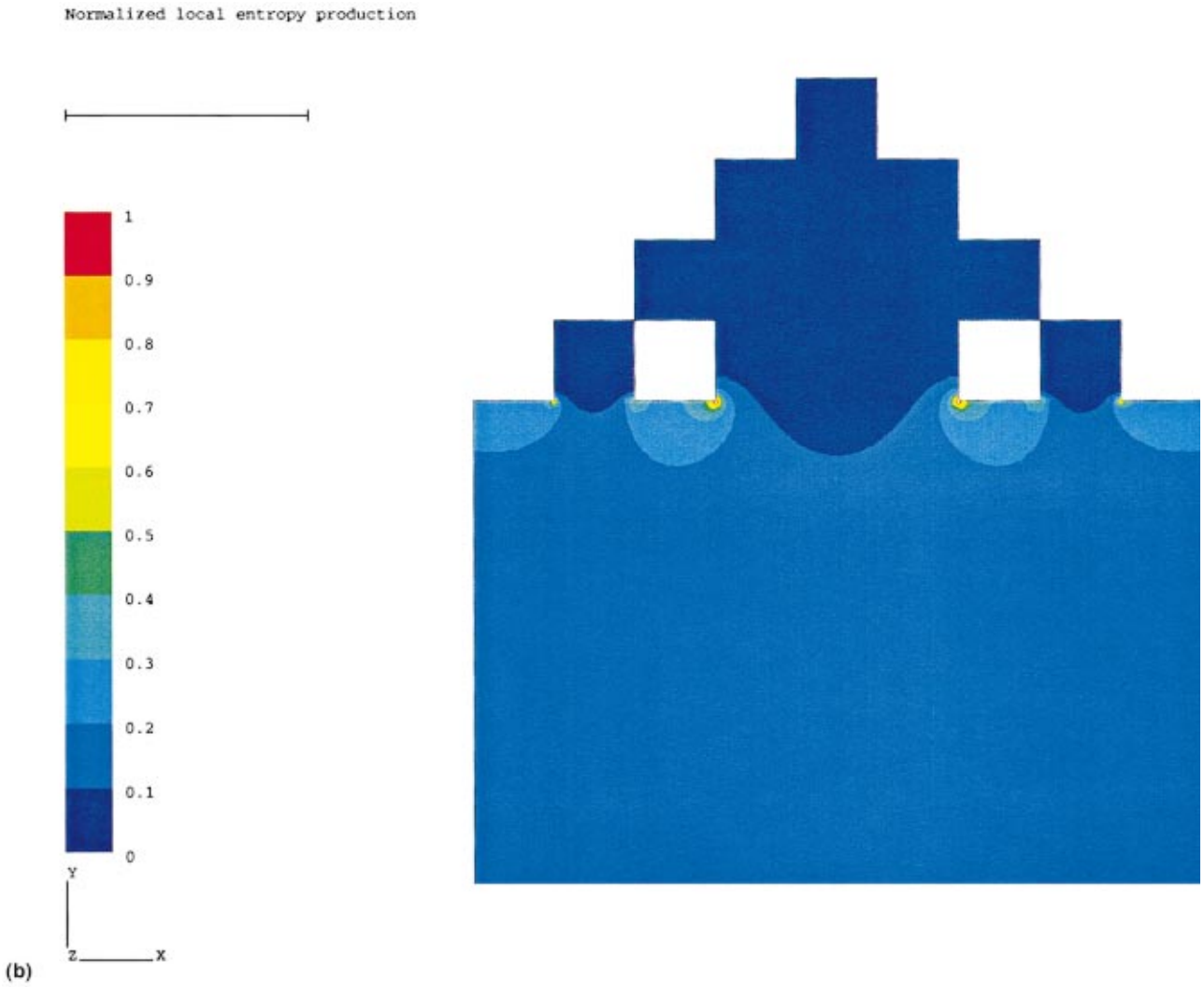

FIG. 5. (*Continued*).

dissipation—are increased. In actual fact, one is here in the presence of a second, adverse factor, related to the fact that a good part of the irregularity is practically inactive from the standpoint of irreversible thermodynamics, on the very grounds of the active zone concept. When these two factors are incorporated into the entropy production the overall balance is, clearly, in favor of the second trend. Our prediction on such dissipation trends should be amenable to experimental testing in a suitably constructed diffusion cell.

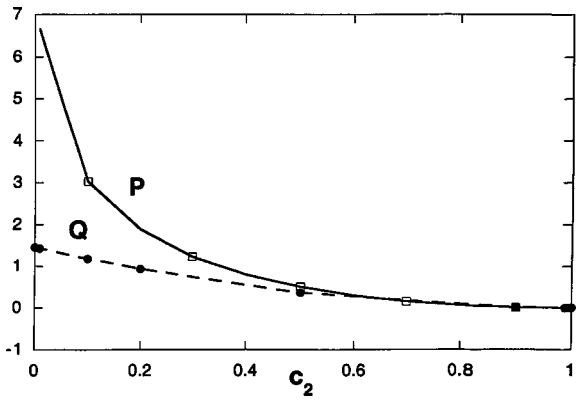

FIG. 6. Variation of the entropy production P normalized by Dk/c_1 (full lines) and of the variational functional Q (dotted lines) as a function of the concentration c_2 in the upper boundary for the first fractal generation. Computer units.

The tendency to decrease dissipation with increasing

TABLE I.

c_2	P (gen. 1)	P (gen. 2)
0.01	6.655	6.603
0.1	3.027	3.006
0.2	1.881	1.868
0.3	1.231	1.223
0.4	0.803	0.798
0.5	0.506	0.503
0.6	0.299	0.296
0.7	0.156	0.155
0.8	6.520[−2]	6.475[−2]
0.9	1.539[−2]	1.529[−2]
0.99	1.468[−4]	1.458[−4]

boundary fragmentation has some potentially interesting repercussions. Especially appealing is the idea that, when viewed from a thermodynamic standpoint, the multitude of the fractal structures encountered in nature appear to display an enhanced efficiency as far as energy transduction is concerned. It would be worthwhile to undertake concrete case studies aiming to implement this point.

Convincing evidence that the mammalian lung is a structure satisfying the principal properties of fractals and, in particular, power-law behavior has been reported by West [21–23]. This author as well as Lefevre [24] have further suggested that such fractal behavior may enhance the organism's stability toward fluctuations or optimize a cost function. These results are consistent with the viewpoint developed in the present work. What is more, dissipation as measured by entropy production offers a natural and physically appealing implementation of Lefevre's idea of a cost function.

The work reported in this paper can be extended along several other directions. The most straightforward one is to consider geometries leading to other fractal structures. A more challenging problem would be to incorporate growth [13,14,21], as, e.g., in diffusion-limited aggregation or viscous fingering related problems, and/or chemical deposition in one of the boundaries.

ACKNOWLEDGMENTS

This work was supported in part by the Pôles d'Attraction Interuniversitaires program of the Belgian Federal Office of Scientific, Technical and Cultural Affairs. Financial support from the Van Buren and Petsalys-Lepage Foundations is also gratefully acknowledged.

[1] C. J. G. Evertsz and B. B. Mandelbrot, J. Phys. A **25**, 1781 (1992).
[2] R. Gutfraind and B. Sapoval, J. Phys. I **3**, 1801 (1993).
[3] B. Sapoval, M. Filoche, K. Karamanos, and R. Brizzi, Eur. Phys. J. B **9**, 739 (1999).
[4] M. Filoche and B. Sapoval, Eur. Phys. J. B **9**, 755 (1999).
[5] N. G. Makarov, Proc. London Math. Soc. **51**, 369 (1985).
[6] P. Jones and T. Wolff, Acta Math. **161**, 131 (1998).
[7] J. Bourgain, Invent. Math. **87**, 477 (1987).
[8] B. Sapoval, *Universilatés et Fractales* (Flammarion, Paris, 1997).
[9] E. R. Weibel, *The Pathway for Oxygen* (Harvard University Press, Cambridge, MA, 1984).
[10] B. J. West, V. Bhargava, and A. L. Goldberger, J. Appl. Physiol. **60**, 1089 (1986).
[11] G. B. West, J. H. Brown, and B. J. Enquist, Science **276**, 122 (1997).
[12] B. B. Mandelbrot, *The Fractal Geometry of Nature* (Freeman, San Francisco, 1982).
[13] T. Vicsek, *Fractal Growth Phenomena* (World Scientific, Singapore, 1989).
[14] M. Schröder, *Fractals, Chaos, Power Laws* (Freeman, New York, 1991).
[15] S. R. de Groot and P. Mazur, *Non-Equilibrium Thermodynamics* (Dover, New York, 1984).
[16] I. Prigogine, *Étude Thermodynamique des Phénomènes Irreversibles* (Desoer, Liège, Belgium, 1947).
[17] C. F. Gerald and P. O. Wheatley, *Applied Numerical Analysis*, 4th ed. (Addison-Wesley, Reading, MA, 1989).
[18] J. Crank, *The Mathematics of Diffusion*, 2nd ed. (Clarendon, Oxford, 1975).
[19] O. C. Zienciewicz, *The Finite Elements Method*, 5th ed. (McGraw-Hill, UK, 2000).
[20] M. E. Laursen and M. Gellert, Int. J. Numer. Methods Eng. **12**, 67 (1978).
[21] A. Hill, Nature (London) **348**, 426 (1990).
[22] B. J. West, Ann. Biomed. Eng. **18**, 135 (1990).
[23] B. J. West, Phys. Rep. **246**, 1 (1994).
[24] J. Lefevre, J. Physiol. **446**, 5788 (1992).